Europe PMC Funders Group
Author Manuscript
*Cell Rep*. Author manuscript; available in PMC 2016 August 12.

Published in final edited form as:
*Cell Rep*. 2015 February 17; 10(6): 968–982. doi:10.1016/j.celrep.2015.01.029.

# Dynamic Co-evolution of Host and Pathogen: HCMV Downregulates the Prevalent Allele MICA*008 to Escape Elimination by NK Cells

**Einat Seidel**[1], **Vu Thuy Khanh Le**[2], **Yotam Bar-On**[1], **Pinchas Tsukerman**[1], **Jonatan Enk**[1], **Rachel Yamin**[1], **Natan Stein**[1], **Dominik Schmiedel**[1], **Esther Oiknine Djian**[3], **Yiska Weisblum**[3], **Boaz Tirosh**[4], **Peter Stastny**[5], **Dana G. Wolf**[3], **Hartmut Hengel**[6], and **Ofer Mandelboim**[1,*]

[1]The Lautenberg Center for General and Tumor Immunology, The Faculty of Medicine, The Hebrew University Medical School, IMRIC, Jerusalem 9112001, Israel

[2]Institute for Virology of the University Hospital Essen, University Duisburg-Essen, 45147 Essen, Germany

[3]Clinical Virology Unit, Hadassah Hebrew University Medical Center and Department of Biochemistry and the Chanock Center for Virology, IMRIC, Jerusalem 9112001, Israel

[4]The Institute for Drug Research, Hebrew University Faculty of Medicine, Hebrew University of Jerusalem, Jerusalem 9112001, Israel

[5]Department of Internal Medicine, UT Southwestern Medical Center, Dallas, TX 75390-8886, USA

[6]Institute of Virology, University Medical Center, Albert-Ludwigs-University Freiburg, Hermann-Herder Strasse 11, Freiburg 79104, Germany

## SUMMARY

Natural killer (NK) cells mediate innate immune responses against hazardous cells and are particularly important for the control of human cytomegalovirus (HCMV). NKG2D is a key NK activating receptor that recognizes a family of stress-induced ligands, including MICA, MICB, and ULBP1-6. Notably, most of these ligands are targeted by HCMV proteins and a miRNA to prevent the killing of infected cells by NK cells. A particular highly prevalent MICA allele, MICA*008, is considered to be an HCMV-resistant “escape variant” that confers advantage to human NK cells in recognizing infected cells. However, here we show that HCMV uses its viral glycoprotein US9 to specifically target MICA*008 and thus escapes NKG2D attack. The finding that HCMV evolved a protein dedicated to countering a single host allele illustrates the dynamic co-evolution of host and pathogen.

This is an open access article under the CC BY-NC-ND license (http://creativecommons.org/licenses/by-nc-nd/4.0/).

*Correspondence: oferm@ekmd.huji.ac.il.

SUPPLEMENTAL INFORMATION

Supplemental Information includes Supplemental Experimental Procedures, six figures, and one table and can be found with this article online at http://dx.doi.org/10.1016/j.celrep.2015.01.029.

Europe PMC Funders Author Manuscripts
Europe PMC Funders Author Manuscripts

Europe PMC Funders Author Manuscripts

Europe PMC Funders Author Manuscripts

## Graphical Abstract

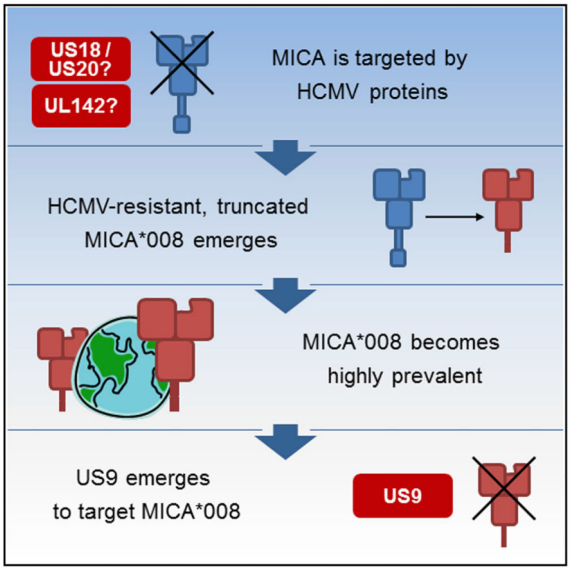


## INTRODUCTION

Human cytomegalovirus (HCMV) is a member of the Betaherpesvirus family, possessing a complex dsDNA genome that encodes hundreds of genes (Stern-Ginossar et al., 2012). The majority of the population is latently infected with HCMV with no overt symptoms, yet HCMV can cause significant morbidity and mortality in immunosuppressed individuals and in congenitally infected neonates (Griffiths, 2012).

Natural killer (NK) cells are innate immune lymphocytes named for their ability to kill cancer cells without prior sensitization (Cheent and Khakoo, 2009). NK cells are especially important in combating viral infections in general and HCMV in particular, and consequently, NK-deficient patients succumb to lethal HCMV infections (Orange, 2013). NK cell activity is governed by integrating signals from a panel of activating and inhibitory receptors (Cheent and Khakoo, 2009). One of the key activating NK receptors is NKG2D, a C-type lectin that recognizes a family of major histocompatibility complex (MHC)-like stress-induced ligands: MHC class I polypeptide-related sequences (MIC) A and B, and UL16 binding proteins (ULBP) 1–6 (Fernández-Messina et al., 2012). NKG2D ligands are usually absent from normal cells, but different forms of stress such as DNA damage and viral infection can induce their expression, leading to recognition and elimination of hazardous cells (Fernández-Messina et al., 2012).

HCMV employs numerous strategies to avoid NK cell recognition (Wilkinson et al., 2008), and many among them target the stress-induced ligands. Specifically, the viral protein UL16 sequesters MICB and ULBP1/2/6 inside infected cells, whereas the viral protein UL142 sequesters MICA and ULBP3 (Halenius et al., 2014; Slavuljica et al., 2011). In addition, the viral glycoproteins US18 and US20 were recently shown to target MICA to lysosomal

Europe PMC Funders Author Manuscripts

Europe PMC Funders Author Manuscripts

degradation (Fielding et al., 2014). Finally, the miRNA HCMV-miR-UL112 targets MICB mRNA to reduce MICB expression (Stern-Ginossar et al., 2007).

MICA is the most polymorphic NKG2D ligand with >80 known alleles (Fernández-Messina et al., 2012). A particular allele, MICA*008, is resistant to various HCMV immune evasion strategies: UL142 does not target it (Ashiru et al., 2009; Chalupny et al., 2006), and it is not downregulated upon infection with HCMV strain AD169 *VarS* (Zou et al., 2005). Unlike most MICA alleles, MICA*008 is truncated and lacks a cytoplasmic tail due to a frameshift mutation in its transmembrane (TM) domain. MICA*008 was recently shown to be glycosylphosphatidylinositol (GPI) anchored, unlike full-length MICA alleles. The GPI-anchoring process is very slow and is mediated by a nonstandard, as yet unknown, pathway (Ashiru et al., 2013).

MICA*008 is the most prevalent allele in most studied populations, comprising up to 53% of all alleles (Petersdorf et al., 1999; Zhang et al., 2001). These findings gave rise to the hypothesis that MICA*008 may confer resistance to HCMV infection, and its high frequency is the result of positive selective pressure exerted by HCMV (Slavuljica et al., 2011; Wilkinson et al., 2008).

The *US2-US11* region of the HCMV genome encodes eight TM glycoproteins of limited homology not essential for HCMV replication in vitro (Huber et al., 2002; Jones and Muzithras, 1991, 1992). Several of these proteins target the MHC pathways, while the function of three others (US7, US8, and US9) remained undetermined (Huber et al., 2002).

Here, we show that US9 selectively downregulates MICA*008, previously thought resistant to HCMV manipulation, to escape NKG2D-mediated attack by NK cells.

## RESULTS

### US9 Selectively Downregulates the Truncated Allele MICA*008

To test whether US7, US8, and US9 modulate NK cell function, we overexpressed them in various cells lines. Because antibodies directed against these HCMV proteins are unavailable, the three proteins were fused to HIS or HA tags. Of the three tested proteins, US7 and US8 had no effect on the expression of the following ligands: MHC class I, β2 m, HLA-E, PVR, Nectin-2, ICAM1, CCM1, MICA, MICB, ULBP1, ULBP2/5/6, and ULBP3 (data not shown). We therefore did not study US7 and US8 any further.

US9 was previously reported to be ER resident (Huber et al., 2002; Mandic et al., 2009). Immunofluorescence revealed a high degree of US9 localization to the ER with no discernible surface expression (Figure S1A). Expression of US9 was also verified by western blotting. As previously shown (Huber et al., 2002), two US9 products, ascribed to different glycosylations, were detected (Figure 1A).

We next tested US9's effect on the surface expression of various NK cell ligands. Notably, expression of US9 in 293T and in HeLa cells abolished MICA expression compared with its level in empty-vector (EV)-transduced controls (Figure 1B). A moderate downregulation of MICA was observed in MCC13 cells, and no MICA downregulation was observed in A549

Europe PMC Funders Author Manuscripts

Europe PMC Funders Author Manuscripts

and in HCT116 cells (Figure 1B). The US9-mediated downregulation of MICA was selective, as no difference was observed in MHC class I and MICB expression (Figure 1B) or in the expression of other stress-induced ligands (Figure S1B).

The selective, cell-type-dependent downregulation of MICA was unexpected. However, because it was previously shown that MICA*008 is resistant to HCMV manipulation (Ashiru et al., 2009; Chalupny et al., 2006; Zou et al., 2005), we speculated that the US9-resistant cells probably express this allele. To our surprise, 293T and HeLa cells were in fact previously shown to be homozygous for MICA*008, whereas HCT116 cells were shown to express full-length MICA alleles (McSharry et al., 2008; Zhang et al., 2001).

We therefore speculated that US9 specifically targets the truncated MICA*008 allele, and to test this, we genotyped the A549 and MCC13 cell lines, which had never been typed. Importantly, we observed a strict correlation between MICA genotype and US9 effect: in the heterozygous MCC13 cells (MICA*008/*009:02), a moderate effect on MICA was observed, and in A549 cells (MICA*001/*004), no effect on MICA expression was observed (Figure 1B). Table S1 summarizes the MICA genotype and expression of the cell lines used in this study.

The main differences between full-length MICA alleles and MICA*008 are shown in Figure 1C. A G-nucleotide insertion at position 952 located in the middle of the MICA*008 TM domain causes a frameshift. This results in an alternate reading frame of 15 amino acids (AAs), followed by a premature stop codon.

## Post-transcriptional Regulation of MICA*008 Expression by US9

To determine the mechanism by which US9 downregulates MICA*008, we performed western blots in the presence or in the absence of US9. It should be noted that MICA is a highly glycosylated protein, which migrates in “smears” due to variable carbohydrate composition (Ashiru et al., 2013). Different exposures of the same gel are shown due to varying MICA expression in the cell lines. A single exposure of the same gel is shown in Figure S2A. Western blots confirmed the cell line genotypes since in the absence of US9, the MICA*008 homozygous cell lines 293T and HeLa express MICA at a size of roughly 60 kDa; the HCT116 cell line, which has full-length alleles, expresses MICA at a size of about 75–100 kDa, while the heterozygous line MCC13 has protein bands of both 75 and 60 kDa (Figure 2A). In the presence of US9, a considerable reduction in MICA*008 level in 293T and HeLa cells was observed (Figure 2A, quantified in Figure 2B). In contrast, in HCT116 cells, no reduction in MICA level was observed. Notably, in the heterozygous MCC13 cell line, only MICA*008 was affected (Figure 2A, quantified in Figure 2B). We validated these results by utilizing HeLa and HCT116 cells transduced with US8 as control (Figure S2B).

These results exclude the possibility that US9 sequesters MICA*008 inside cells. To investigate whether US9 affects MICA*008 mRNA quantity, we performed qRT-PCR on cDNA extracted from HeLa cells (MICA*008 homozygous) and from MCC13 cells (heterozygous) and observed no significant differences (Figure 2C). This suggests that US9 acts post-transcriptionally.

Europe PMC Funders Author Manuscripts

Europe PMC Funders Author Manuscripts

We confirmed these results in RKO cells, which express very low levels of the full-length allele MICA*007:01 (Table S1; Figures 2D and S2C). We transduced RKO cells either with the full-length allele MICA*004 or with MICA*008, fused to an N-terminal HA tag, and then co-transduced these cells with EV or with US9 fused to a HIS tag. MICA*008 levels were substantially reduced in US9-expressing cells compared with the EV control (Figure 2D), while no difference was apparent in MICA*004 expression. We validated these results by blotting with an α-HA tag antibody (Figure 2E) and by comparing to EV, US7, and US8-expressing controls (Figure S2C). Immunofluorescent imaging of the RKO transfectants showed that MICA*008 indeed almost vanished from the US9-expressing cells (Figure 2F).

## US9 Targets MICA*008 to Proteasomal Degradation

Intriguingly, in RKO transfectants, all MICA alleles migrated at a higher molecular weight, MICA*004 at ~100 kDa and MICA*008 at ~70 kDa, probably due to altered glycosylations. Concurrently, another MICA*008 form of ~60 kDa could be detected in RKO cells, and this form of the protein was unaffected by US9 (indicated by an arrow; Figures 2D, 2E, and S2C), suggesting that some forms of MICA*008 may be US9 resistant and that US9 acts post-translationally.

To analyze the mechanism by which US9 affects MICA*008, we digested with endoglycosidaseH (endoH) and PNGaseF lysates obtained from HeLa cells (endogenous MICA*008) and from RKO-MICA*008-HA transfectants (Figures 3A–3D, respectively) in the presence of EV or US9. In HeLa-EV cells (Figure 3A), most MICA*008 was endoH resistant. Deglycosylation with PNGaseF revealed two distinct bands: a band of 37 kDa, representing the endoH sensitive, non-GPI-anchored form of MICA*008, and a band of about 34 kDa, representing the endoH resistant, GPI-anchored form of MICA*008 (Ashiru et al., 2013). In contrast, in HeLa-US9, only the endoH-sensitive, 37-kDa form of MICA*008 remained (Figure 3B).

In RKO cells, deglycosylation revealed that the highly glycosylated band that migrates at ~70 kDa corresponds to the mature, GPI-anchored 34-kDa form of MICA, whereas the ~60-kDa US9-resistant band corresponds to the endoH-sensitive, 37-kDa form of MICA. Similar to what was seen in HeLa cells, only the 37-kDa form of MICA*008 could be detected in the presence of US9. Following PNGaseF treatment, it was also possible to detect a fainter band of ~42 kDa, which represents the deglycosylated native full-length allele expressed by RKO cells (Figures 3C and 3D).

These observations suggest that US9 does not act on MICA*008 while it is in its non-GPI-anchored form, but still targets it prior to its egress from the ER, since no endoH-resistant forms of MICA*008 could be detected in US9-expressing cells. Along with the fact that US9 is ER resident (Figure S1A), this implied that US9 acts by recruiting ER-associated degradation (ERAD) complexes, which dislocate proteins from the ER lumen to the cytosol, where the proteins are deglycosylated and degraded by the proteasome (Loureiro and Ploegh, 2006).

To test this hypothesis, HeLa cells expressing either EV (Figure 3E) or US9 (Figure 3F) were treated for 16 hr with several inhibitors of lysosomal or of proteasomal degradation or

Europe PMC Funders Author Manuscripts

Europe PMC Funders Author Manuscripts

with an appropriate mock treatment and then lysed and immunoblotted to find whether any of these treatments would increase MICA*008 levels in US9-expressing cells. Prolonged treatments were required to show an effect, presumably due to MICA*008's slow maturation kinetics (Ashiru et al., 2013). In EV-expressing HeLa cells (Figure 3E), the proteasome inhibitors, as well as concanamycin A (CCM A), a lysosomal acidification inhibitor, induced MICA expression. All inhibitors also upregulated MICA in US9-expressing cells (Figure 3F). However, we cannot discern whether it is due to MICA induction (which may differ in its extent between EV- and US9-expressing cells) or due to inhibition of MICA degradation. Nevertheless, in the US9-expressing cells, a smear of MICA*008 forms of sizes down to 37 kDa (the size of the deglycosylated non-GPI-anchored form of MICA*008) appeared following treatment with the proteasome inhibitors epoxomicin (EPX), bortezomib (BTZ), and MG132 (Figure 3F, indicated by arrows). We hypothesized that these forms represent deglycosylated cytosolic degradation intermediates, reminiscent of MHC class I heavy chain degradation by US2. In another intriguing parallel to US2, US9 itself is subject to proteasomal degradation, since its levels are increased in the presence of proteasome inhibitors (Figure 3F) (Wiertz et al., 1996).

To prevent interference from MICA induction, we utilized cycloheximide (CHX) chase, which isolates protein degradation rate. We treated HeLa-EV (Figure 3G) or HeLa-US9 (Figure 3H) cells with inhibitors of proteasomal or lysosomal degradation, in combination with CHX, for 8 hr. This treatment prevented the induction of MICA*008, and importantly, in US9-expressing cells treated with proteasome inhibitors, 37-kDa degradation intermediates of MICA*008 appeared again (Figure 3H, arrow). No effect was observed in EV-expressing cells (Figure 3G) or for lysosomal inhibitors.

We validated these results by performing an 8-hr CHX chase in RKO-MICA*008-HA transfectants, which co-express EV (Figure S3A) or US9 (Figure S3B) in the presence of different doses of proteasome and lysosome inhibitors. As expected, the quantity of the ~60-kDa immature form of MICA was greatly reduced following prolonged CHX treatment in EV and US9-expressing cells. In US9-expressing cells (Figure S3B), this reduction was partially rescued only by proteasome inhibitors treatment, which also led to the dose-dependent appearance of 37-kDa degradation intermediates of MICA*008 (Figure S3B, arrows). In contrast, the inhibitors did not affect EV-expressing cells (Figure S3A).

Because the reduction in the ~60-kDa MICA form quantity was mitigated by proteasome inhibitors in CHX-treated, RKO-MICA*008-HA US9-expressing cells, we wanted to study the composition and maturation status of this form following proteasome inhibitor treatment. To this end, RKO-MICA*008-HA cells expressing EV (Figure S3C) or US9 (Figure S3D) were left untreated or were treated with a combination of CHX and DMSO (mock) or with a combination of CHX and proteasome inhibitor EPX. Cells were lysed, and lysates were untreated or digested with endoH or PNGaseF. Results revealed that the 37-kDa non-GPI-anchored, endoH-sensitive form of MICA*008 is increased in quantity following EPX treatment in US9-expressing cells (Figure S3D), in accordance with the hypothesis that it is targeted by US9 to proteasomal degradation.

Europe PMC Funders Author Manuscripts

Europe PMC Funders Author Manuscripts

## Specific Features of MICA*008, Correlated with Noncanonical GPI Anchoring, Are Required for US9-Mediated Downregulation

MICA*008 has two distinguishing features compared with full-length alleles: a unique 15-AA sequence in the TM region and an absent cytoplasmic domain. To determine which feature is important for the specific targeting of MICA*008 by US9, we generated several mutations in the full-length MICA*004 protein (Figure 4A) and examined which of these would recapitulate the MICA*008 phenotype upon co-expression with US9. For these experiments, we again used RKO cells transfected with different MICA alleles co-expressing an EV or US9. The native full-length MICA allele of RKO cells was undetected at the cell surface (Figure 4B, left-most histogram). In agreement with our aforementioned western blot results (Figures 2D and 2E), US9 did not affect the surface expression of the full-length allele MICA*004-HA but substantially reduced the levels of MICA*008-HA as assayed by fluorescence-activated cell sorting (FACS) staining with α-MICA antibody (Figure 4B) and α-HA tag antibody (Figure S4A). Next, we introduced a G-insertion mutation (characteristic of MICA*008), which leads to an altered reading frame of 15 AA and a premature stop codon (Figure 4A) into MICA*004-HA. The resultant mutant, MICA*004-G-ins-HA, still differs from MICA*008 in extracellular domain polymorphisms. Despite this, MICA*004-G-ins-HA was robustly downregulated by US9 (Figures 4B and S4A).

To test whether the absence of the cytoplasmic tail in MICA*008 is responsible for the US9-mediated downregulation, a premature stop codon was introduced in MICA*004 (MICA*004-stop-HA) at the end of the TM domain, but without the G-insertion mutation (Figure 4A). The resultant MICA*004-stop-HA protein was not downregulated by US9 (Figures 4B and S4A). We then tested whether the 15-AA sequence was itself sufficient for US9 recognition and generated a MICA*004 protein, named MICA*004-Dmut-HA, containing the 15 AAs found in MICA*008 and also including a second mutation to restore the reading frame and the cytoplasmic domain (Figure 4A). Because cells expressing MICA*004-Dmut-HA were also unaffected by US9 (Figures 4B and S4A), we concluded that both the absence of the cytoplasmic domain and the presence of the unique 15-AA sequence in the TM region of MICA*008 were necessary for US9 recognition. We verified our results by immunoblotting lysates obtained from the same cells described above. The absence of the mature form of MICA in the presence of US9 was observed only in MICA*008-HA and in MICA*004-G-ins-HA (Figure S4B), in accordance with the flow cytometry results.

To characterize whether the MICA mutants we created are GPI-anchored, like MICA*008, we treated RKO cells transduced with the various MICA constructs for 2 hr with phosphatidylinositol-specific phospholipase C (PI-PLC), which specifically cleaves GPI anchors, and then assessed the surface expression of MICA. Staining for ULBP3, a GPI-anchored stress-induced ligand, served as a positive control. Only MICA*008-HA and MICA*004-G-ins-HA, the proteins susceptible to US9, were also affected by PI-PLC treatment (Figure 4C). MICA surface levels were reduced to a lesser extent by the treatment compared with ULBP3, in accordance with previous results regarding MICA*008, attributed to fatty-acid modifications of the inositol moiety, which can hamper PI-PLC activity (Ashiru

Europe PMC Funders Author Manuscripts

Europe PMC Funders Author Manuscripts

et al., 2013). We verified this result by digesting lysates from RKO cells transduced with the constructs described in Figure 4A with PNGaseF. Only lysates from MICA*008-HA and MICA*004-G-ins-HA migrated as two distinct bands, due to the addition of the GPI moiety (Figure S4C).

Because our initial mutant screen revealed a correlation between the GPI-anchoring status of the MICA mutants and US9's ability to downregulate it, the question arose whether US9 might simply recognize MICA, which undergoes GPI anchoring. To address this, we generated an additional chimeric protein, named MICA*008-ULBP3TM-HA, where we swapped MICA*008's TM domain with that of ULBP3, which contains a canonical GPI-anchoring signal (Figure 4A). The resultant chimera was indeed GPI anchored and susceptible to PI-PLC treatment like ULBP3 itself (Figure 4C), although we were not able to observe two distinct bands following PNGaseF digestion of MICA*008-ULBP3TM-HA (Figure S4C), probably due to its faster maturation (Fernández-Messina et al., 2012). Despite this, US9 did not downregulate MICA*008-ULBP3TM-HA (Figures 4B and S4A), indicating that some feature unique to MICA*008's sequence or processing is required for US9-mediated downregulation.

To confirm our conclusions, we swapped the TM domain of MICB, which is not targeted by US9 (Figure 1B), with the TM domain and the premature stop codon of MICA*008 (Figure 4D) to create a chimeric protein termed MICB-mut. A full-length MICB*002 allele, or the chimeric MICB-mut, was introduced into 293T cells, which lack MICB surface expression (as seen in Figure 4E), and the cells were then co-transduced with US9 or with an EV. Low levels of MICB-mut-HA were expressed on the cell surface, probably because of the swapping of its TM domain. In contrast to the full-length MICB, which is unaffected by US9, the chimeric MICB-mut was indeed susceptible to US9 (Figure 4E).

## A Common US9 Variant with a C-Terminal Deletion Is Functional against MICA*008

US9 is a highly conserved protein, apart from a variant present in many HCMV strains, which lacks 15 AAs at its C terminus, resulting in a protein of 232 AAs instead of 247 AAs (Mandic et al., 2009). Sequence alignment of representative US9 sequences is shown in Figure S4D. We therefore wondered whether the C-truncated 232-AA form of US9 is functional against MICA*008. We inserted the C terminus deletion into the US9 protein of the TB40 strain and transduced it into RKO cells expressing MICA*004-HA or MICA*008-HA. Because the 232-AA variant of US9 caused downregulation of MICA*008 similar to the full-length variant of US9 and had no effect on MICA*004 (Figure S4E), we concluded that the C terminus of US9 is redundant for its downregulation of MICA*008 and that this common variant is fully functional.

## US9 Downregulates MICA*008 during HCMV Infection

We next investigated whether US9 downregulates MICA*008 during HCMV infection. For this purpose, primary human foreskin fibroblasts (HFFs) were obtained from several healthy donors and genotyped for MICA. The HFFs termed VH3 (Hengel et al., 1995) were homozygous for MICA*008, while the HFFs termed FLS1 (MICA*004/*009:01-*049; the latter alleles differ in a single nucleotide in exon 6 and could not be distinguished) were used

Europe PMC Funders Author Manuscripts

Europe PMC Funders Author Manuscripts

as controls (Table S1). We generated a mutant lacking *US9* (ΔUS9) on the background of HCMV strain AD169 *VarL*, which contains most of the UL*b′* genomic region lacking in AD169 *VarS*, but harbors a *UL140-UL144* deletion. Consequently, this virus lacks UL142, which targets MICA full-length alleles and ULBP3. We verified that *US9* is not present in the viral genome and is not expressed during infection (Figures 5A and S5A, respectively).

Next, we infected the VH3 and FLS1 cells with the WT AD169- *VarL* virus or with the ΔUS9 virus at an MOI of 2–4 and performed time-course assays to track MICA surface expression from 0-hr postinfection (hpi) to 72 hpi (Figure 5B). In the FLS1 HFF (full-length alleles), MICA surface expression was progressively downregulated until it was abrogated at 72 hpi, with no difference observed between the WT and ΔUS9 viruses. Importantly, in the VH3 HFFs (MICA*008), the WT virus was able to downmodulate MICA, while the ΔUS9 virus was significantly impaired in MICA downregulation. At 72 hpi in the ΔUS9-infected VH3 cells, MICA*008 expression was 2.5- to 3-fold higher than in the WT-infected cells (Figure 5C). It is interesting to note that even the WT virus was unable to abolish MICA*008 expression, while it was able to abolish MICA*004 expression. However, in this system, MICA levels are also influenced by the induction of MICA expression caused by HCMV infection (Fielding et al., 2014; Zou et al., 2005).

To validate these results in a system with constant MICA levels, we next expressed different MICA alleles in primary HFF. For these experiments, we used HFF termed FLS3, which we observed in our screening to completely lack MICA protein expression (Figures 5D and 7A), despite expressing MICA at the mRNA level (Table S1). We transduced the FLS3 cells with an EV, with MICA*004-HA or with MICA*008-HA, and infected them with the WT or ΔUS9 viruses at an MOI of 2–4. At 72 hpi, in the MICA*004-HA-expressing transfectants, both WT and ΔUS9 viruses were able to reduce MICA surface expression to about 2%–3% of the uninfected (UI) level (Figure 5D, quantified in Figure 5E). Conversely, in the MICA*008-HA transfectants, while MICA surface levels were decreased in the ΔUS9-infected cells compared with the UI controls, they were significantly higher than those in the WT-infected cells, again resulting in a roughly 2.5-fold increase (Figure 5D, quantified in Figure 5E). Interestingly, the WT virus was once more impaired in reducing MICA*008 expression, reducing its levels only to about 15% of the original levels, and the absence of US9 was not sufficient to completely restore MICA*008 expression, implying that other viral mechanisms also downregulate this allele.

To confirm these results during infection with a viral strain, which retains the clinical strain characteristics, we infected FLS1, VH3, and FLS transfectants with TB40/E-pp150-GFP (Figure S5B). TB40/E behaved in the same way as the AD169 *VarL* virus: it completely downregulated full-length MICA alleles, but not MICA*008. To validate the specificity of US9 during HCMV infection, we stained the infected FLS1, VH3, and FLS3 transfectant cells for additional stress-induced ligands at 72 hpi (Figure S5C). As expected, both ULBP1 and ULBP2 were downregulated upon HCMV infection, whereas ULBP3 was upregulated, possibly because AD169 *VarL* lacks UL142. No differences were observed between WT and ΔUS9-infected cells.

Europe PMC Funders Author Manuscripts

Europe PMC Funders Author Manuscripts

### The US9-Mediated Downregulation of MICA*008 Resulted in Reduced NKG2D-Dependent NK Killing in US9 Overexpression and during HCMV Infection

We next asked whether the US9-mediated reduction of MICA*008 expression would affect NK-mediated killing. For this purpose, we performed a killing assay in which $^{35}$S-labeled cells expressing an EV or US9 were co-incubated for 5 hr with primary bulk activated NK cells, in the presence and in the absence of a blocking α-NKG2D monoclonal antibody (mAb) (Figures 6A and 6B). We began with HCT116 cells, which only express full-length MICA alleles, and found no significant differences between the killing of EV-expressing cells and US9-expressing cells (Figure 6A). When NKG2D was blocked, the killing of HCT116 cells expressing US9 or EV was similarly reduced (Figure 6A). In contrast, the MICA*008-homozygous 293T cells expressing US9 were killed less efficiently than EV-expressing cells in the absence of treatment or in the presence of a control antibody (12E7; Figure 6B). Blocking of NKG2D eliminated these differences, and the killing of all 293T cells was similar (Figure 6B), indicating the specific US9-induced abrogation of MICA*008 expression resulted in reduced NKG2D-mediated killing. It should be noted that NKG2D blocking significantly reduced the killing even in US9-expressing 293T cells, presumably because these cells express other stress-induced ligands (Figure S1B).

We proceeded to test whether the increase in MICA*008 surface expression in ΔUS9-infected cells would lead to increased NK-mediated killing during HCMV infection. For this purpose, we utilized FLS1 fibroblasts, which express full-length alleles, and VH3 fibroblasts, which only express MICA*008. The fibroblasts were UI or infected with the WT AD169 *VarL* virus or with the ΔUS9 mutant. At 72 hpi, the $^{35}$S-labeled cells were co-incubated overnight with primary bulk activated NK cells (Figures 6C and 6D). The NK cells were left untreated, were treated with a control mAb (12E7), or were treated with an NKG2D-blocking mAb. FLS1 cells were poorly killed, and no significant differences were observed in killing under all conditions and treatments (Figure 6C). Importantly, there were no differences between WT- and ΔUS9-infected cells under any treatment. VH3 cells were also poorly killed; however, in contrast to FLS1 cells, the killing was significantly higher in the ΔUS9-infected cells compared with the WT-infected cells, and this difference was abrogated when NKG2D was blocked (Figure 6D).

We repeated this experiment in FLS3 HFF transduced with EV, MICA*004-HA, or MICA*008-HA (Figures S6A–S6C). FLS3-EV cells were poorly killed under all conditions (Figure S6A), but transduction with MICA*004-HA and MICA*008-HA dramatically increased killing efficiency. Blocking with α-NKG2D significantly reduced the killing of MICA*004-HA and MICA*008-transfected cells across all conditions (Figures S6B and S6C). In FLS3-MICA*004-HA cells, HCMV infection significantly reduced the killing, but no difference was observed between cells infected with the WT virus or with the ΔUS9 mutant under any treatments (Figure S6B). Importantly, in FLS3-MICA*008-HA cells, the killing was significantly higher in the ΔUS9-infected fibroblasts compared with the WT-infected fibroblasts, and NKG2D blocking abrogated this difference (Figure S6C). These results indicate that US9 is functional in reducing NKG2D-mediated killing during HCMV infection.

Europe PMC Funders Author Manuscripts

Europe PMC Funders Author Manuscripts

### US9 Reduces the Amount of GPI-Anchored MICA*008 in HCMV-Infected Cells but Does Not Affect Overall MICA*008 Levels

Finally, we asked whether US9 employs the same mechanism during HCMV infection as in overexpression. To address this question, we infected FLS3 transfectants with WT or ΔUS9 viruses at an MOI of 2–4 or left them UI. Cells were lysed at 72 hpi and analyzed by western blot (Figure 7A). Surprisingly, despite large differences in the surface expression of MICA*008 between WT and ΔUS9-infected cells, we saw no differences in MICA*008 levels in the whole-cell lysates. Similar results were obtained using FLS1 and VH3 HFFs (Figure 7B). In VH3 HFFs, MICA*008 levels in whole-cell lysates were dramatically increased compared with the UI control, both in WT and in ΔUS9-infected cells. Notably, MICA*008 migrated at a lower kDa (~55 kDa) in the HCMV-infected cells compared with the UI controls (~60 kDa). We therefore subjected lysates from FLS3 MICA*008-HA cells (Figure 7C, quantified in Figure 7D) and from VH3 cells (Figure 7E, quantified in Figure 7F) to digestion by endoH and PNGaseF. In UI cells of both kinds, the 34-kDa GPI-anchored endoH-resistant form of MICA*008 was the most abundant. But following infection, the 37-kDa, endoH-sensitive, non-GPI-anchored form of MICA*008 became the most prevalent. The effect was especially pronounced in VH3 cells where this form greatly accumulated (Figure 7E), probably due to the upregulation of the endogenous MICA*008 allele following HCMV infection. The 34-kDa GPI-anchored form was reduced in the HCMV-infected cells, but less so in the ΔUS9-infected cells. There was a 2- to 5-fold increase in the 34-kDa form of MICA (Figures 7D and 7F). Since the 34-kDa form of MICA*008 is the form found at the cell surface (Ashiru et al., 2013), this difference accounts for the decreased FACS staining of MICA*008 in ΔUS9 versus WT-infected cells (Figures 5B–5E).

Since only a small proportion of the total quantity of MICA*008 seemed to be affected by US9, we could not analyze the effect of proteasome inhibitors in the context of HCMV infection (data not shown).

As it was apparent that a viral mechanism is inducing the accumulation of MICA*008 in an endoH-sensitive form, which indicates that MICA*008 is retained inside the ER, we sought to verify this by immunofluorescence. UI, WT-infected, or ΔUS9-infected FLS3-MICA*008-HA transfectants were fixed and stained for MICA and for protein disulfide isomerase (PDI), an ER marker, at 72 hpi. The results showed a substantial merge between MICA*008 and PDI both in WT and in ΔUS9-infected cells, corresponding to a 2-fold increase in the correlation coefficient between the two markers compared with UI controls (Figure S6D). This supports the conclusion that MICA*008 is retained inside the ER during HCMV infection by a viral mechanism other than US9.

## DISCUSSION

The importance of the NKG2D ligands in HCMV immune control has become increasingly clear in the past few years, with the discovery of interlaced viral immune evasion mechanisms targeting these ligands at multiple checkpoints. Because NKG2D is expressed both on NK and on $CD8^+$ T cells, targeting its ligands is doubly advantageous for the virus. These mechanisms parallel in their complexity the HCMV mechanisms that target the MHC

Europe PMC Funders Author Manuscripts

Europe PMC Funders Author Manuscripts

pathways of antigen presentation at multiple stages: proteasomal degradation of the MHC heavy chain (US2 and US11), retention of MHC heavy chains in the ER (US3), and disruption of peptide processing and transport to prevent peptide loading (US6 and the viral miRNA miR-US4-1) (Halenius et al., 2014). Similarly, at least four HCMV proteins, as well as a viral miRNA, all act together to prevent NKG2D ligand expression, by means which include protein sequestration, translational inhibition, and protein degradation.

Against this wealth of diverse viral immune evasion mechanisms, the existence of the "escape variant" MICA*008 was seen as exemplifying the evolutionary process, which led to the diversification of NKG2D ligands in the race against viruses (González et al., 2008; Slavuljica et al., 2011). Our findings show that this often-cited example is in fact only a piece of the jigsaw. It is tempting to speculate that US9 specifically targets this unique MICA allele and constitutes a viral adaptation to the emergence of MICA*008. The specificity of US9 for MICA*008 and not for other MICA alleles illustrates its importance.

Here, we demonstrate that US9 targets MICA*008 to proteasomal degradation, in a manner peculiarly reliant on MICA*008's maturation process. First, the quantity of ER-resident, non-GPI-anchored MICA*008 is not substantially changed in US9-expressing cells. This indicates that US9 does not target MICA*008 as soon as it is synthesized. Instead, the kinetics of US9's effect on MICA*008 are slow, as shown by CHX chase, mirroring MICA*008's own slow maturation process (Ashiru et al., 2013) and implying the US9 is dependent on a certain lag in this process before it can act. US9's dynamics vary from those of US2 and US11, which act within minutes of MHC heavy-chain synthesis (Loureiro and Ploegh, 2006). Finally, US9 susceptibility requires specific features of MICA*008 that are correlated with GPI anchoring status. At the same time, GPI anchoring via the canonical pathway does not confer US9 susceptibility on MICA. Overall, these results indicate that it is the nonstandard GPI-anchoring pathway of MICA*008 that is required for US9's activity. Involvement by constituents unique to MICA*008's nonstandard pathway would also account for US9's inability to target other canonically anchored stress-induced ligands such as ULBP3.

The finding that US9 targets MICA*008 was very surprising since HCMV was considered ineffectual against this allele. There are several possible explanations as for why the effect was not noticed, most notably that MICA*008 downmodulation is less efficient than that of the full-length alleles and might have been overlooked. This is especially true in the study of native MICA alleles, which are concomitantly induced during infection, creating the misleading appearance that no change has occurred compared with UI controls. Another explanation is that only western blots were used to assess HCMV's effect on MICA, and this method may not reveal US9's effect, as we ourselves have observed.

Although US9 efficiently reduces cellular MICA*008 levels in overexpression settings, we could not observe such differences during HCMV infection. There are two possible reasons for this discrepancy: the first is that US9 acts by a different mechanism during infection, sequestering MICA*008 in the ER rather than degrading it. Although possible, we consider the second explanation more plausible: that US9's effect on MICA*008 overall protein quantity is masked by an additional viral mechanism(s). Such a masking effect is not

Europe PMC Funders Author Manuscripts

Europe PMC Funders Author Manuscripts

uncommon when multiple proteins act on the same target. For instance, the full effect of US18 and US20 on MICA could only be demonstrated during infection by deleting both of them (Fielding et al., 2014). Hence, it is not trivial that we were able to demonstrate US9's effect on MICA*008 even in the presence of these other viral mechanisms.

These mechanisms act at least in part by retaining MICA*008 in the ER, as shown by the accumulation of endoH-sensitive MICA*008 and by its colocalization with an ER marker in HCMV-infected cells. Taken together with our findings regarding US9's mechanism of action, we propose the following model for HCMV's effect on MICA*008 (Figure 7G): HCMV infection upregulates the mRNA levels of MICA*008, resulting in increased translation. To counter this upregulation, an unknown viral mechanism(s) binds the newly synthesized MICA*008 and sequesters it inside the ER. Only MICA*008, which eludes these mechanisms, undergoes GPI anchoring, via an unknown noncanonical pathway. US9 targets this stage and diverts MICA*008 to the cytosol, where it is subsequently degraded by the proteasome. This model postulates that, like the HCMV mechanisms targeting MHC, the mechanisms that target MICA*008 also act on distinct stages in its maturation. If these mechanisms act at an earlier stage than US9 does, it would explain why US9 seems to affect only a small proportion of MICA*008 in HCMV-infected cells, as well as why US9's effect was not completely masked by the other viral mechanism(s).

Additional studies are required to elucidate this point. In particular, characterization of the unknown viral mechanism(s) and study of US9's function in their absence is required to settle the question of US9's mechanism of action during infection. Additional research is also required to shed light on additional aspects of US9's function, and in particular the role of MICA*008's GPI-anchoring pathway in it. Another open question is US9's cellular localization: studies, our own included, which found US9 to be ER localized based on immunofluorescence and endoH sensitivity, utilized US9 overexpression to determine its localization (Huber et al., 2002). It is possible that in the context of HCMV infection US9 reaches the plasma membrane, as shown by Weekes et al. (2014) by mass spectrometry. If true, the meaning of this altered localization pattern remains to be determined.

Although we have found that at least two viral mechanisms target MICA*008, based on HCMV's reduced ability to downregulate MICA*008 compared with full-length alleles, we suggest that the viral countermeasures targeting MICA*008 are still fewer and/or less efficient than those targeting full-length alleles. While the question of whether US18 and US20 target MICA*008 has yet to be addressed, we speculate that they do not target this allele, or do so with low efficiency. Overall, these findings support the hypothesis that US9 is a recent addition to HCMV's arsenal, which has yet to fully adapt to the emergence of MICA*008. Indeed, US9 is relatively new in CMV evolution: US9 is less conserved than other US2–US11 family members that target the MHC family (Pande et al., 2005) and less conserved than the MICA-targeting proteins US18 and US20 (Fielding et al., 2014), all of which have homologs in Rhesus CMV. Similarly, MICA*008 has also evolved recently (Fukami-Kobayashi et al., 2005). Furthermore, humans are the only species known to encode a truncated allele of MICA (Pellet et al., 1999).

Europe PMC Funders Author Manuscripts

Europe PMC Funders Author Manuscripts

We therefore propose the following event sequence: MICA was initially targeted by HCMV proteins, such as UL142 and/or US18 and US20. Subsequently, the truncated allele MICA*008 emerged and, due to its ability to escape HCMV control, conferred a selective advantage and became very prevalent. As a response, US9 arose to target MICA*008, perhaps as a duplication or adaptation of an ancestor US2–US11 family member. This example illustrates the dynamic and ongoing co-evolution of virus and host, which enables the former to be so exquisitely tailored to the latter.

## EXPERIMENTAL PROCEDURES

### Cells and Antibodies

The 293T (CRL-3216), RKO (CRL-2577), HeLa (CCL-2), A549 (CCL-185), and MCC13 cell lines were used. All cell lines were obtained from the ATCC except MCC13 cells, which were the kind gift of J.C. Becker (Medical University of Graz, Austria). Human fibroblasts were obtained from primary cultures of foreskins from healthy donors. VH3 fibroblasts were described previously (Hengel et al., 1995). FLS1 and FLS3 fibroblasts were the kind gifts of Professor F. Levi-Schaffer (Hebrew University of Jerusalem). HFFs were used below passage 20. NK cells were isolated from peripheral blood lymphocytes (PBL) samples and activated as previously described (Mandelboim et al., 1996). NK purity was >95% by FACS analysis. All primary cells were obtained in accordance with the institutional guidelines and permissions for using human tissues. Culture conditions and a list of antibodies used in this study appear in the Supplemental Experimental Procedures.

### Lentiviral Constructs, Production, and Transduction

Lentiviruses were generated in 293T cells using a transient three-plasmid transfection protocol as previously described (Stern-Ginossar et al., 2007). Transduction efficiency was assessed by GFP or by surface expression, and only cell populations with >90% efficiency were used for experiments. Where necessary, limiting dilution or cell sorting was used. A detailed description of primers and templates used for cloning and PCR mutagenesis is included in the Supplemental Experimental Procedures.

### Viruses

The US9 deletion mutant (ΔUS9) was generated using the BAC-cloned AD169-*var*L genome pAD169 (Le et al., 2011) as parental. Details of mutant generation and procedures for viral infection are described in the Supplemental Experimental Procedures. The virus strain TB40/E-pp150-GFP was generously provided by C. Sinzger.

### Cytotoxicity Assays and NK Cell Preparation

The cytotoxic activity of NK cells against various targets was assessed in $^{35}S$ release assays as described (Mandelboim et al., 1996) and incubated for 5 hr overnight. The final concentration of the blocking antibodies was 0.5–1.0 μg per well. The spontaneous release in all assays was always less than 50% of the total release and is subtracted from the calculation of the percentages of lysis. Percentages of killing were calculated as follows: (counts per minute [CPM] sample − CPM spontaneous)/(CPM total − CPM spontaneous) × 100.

Europe PMC Funders Author Manuscripts

Europe PMC Funders Author Manuscripts

### Western Blot Analysis

Cells were plated at an equal density, incubated overnight, and lysed in buffer containing 0.6% SDS and 10-mM Tris (pH 7.4). In certain cases, lysates were digested with endoglycosidase H (endoH) or PNGaseF (NEB), according to the manufacturer's instructions. Quantification of blots was performed with the Image Lab software.

### qRT-PCR

Details of the qRT-PCR procedure and the list of primers are included in the Supplemental Experimental Procedures.

### Immunofluorescence

Cells were grown on glass slides and fixed and permeabilized in cold (−20°C) methanol. Cells were blocked overnight in CAS-block (Life Technologies) and then incubated overnight with primary antibodies diluted 1:50–200 in CAS block; they were then washed and incubated overnight in secondary antibodies diluted 1:500 in 5% BSA PBS. Cells were then washed, treated for 5 min with DAPI, and covered with coverslips. A confocal laser scanning microscope (Olympus Fluoview FV1000) was used to obtain images. Co-localization was calculated using the Olympus FluoView FV1000 software.

### Flow Cytometry

For flow cytometry, cells were plated at equal densities and incubated overnight. Resuspended cells were incubated on ice for 1 hr with the primary antibody at a concentration of 0.2 μg/well. The cells were then incubated for 30 min on ice with the appropriate secondary antibody at a concentration of 0.75 μg/well. In all experiments using cells transduced with a GFP-expressing lentivirus, the histograms are gated on the $GFP^+$ population.

### Proteasome and Lysosome Inhibition and CHX Chase

For proteasome and lysosome inhibition, cells were incubated for 16 hr with mock treatment or with the following inhibitors: EPX (Merck Millipore), MG132 (Merck Millipore), BTZ (LC Biolabs), leupeptin (LEU; Merck Millipore), or CCM A (Merck Millipore). For proteasomal and lysosomal inhibition during CHX chase, cells were left untreated or were incubated for 8 hr in the presence of CHX (50–100 μg/ml; Sigma-Aldrich) in combination with the aforementioned inhibitors or with mock treatment. In all experiments, mock-treated cells were treated with equivalent concentrations of DMSO or double-distilled water (DDW).

### PI-PLC Treatment

Cells were incubated for 2 hr with 2 U/ml phosphatidylinositol-specific phospholipase C (PI-PLC; Sigma-Aldrich), and flow cytometry was performed as described.

### Statistical Methods

For statistical significance, Student's t test analysis was used. A statistical test was considered significant when $p < 0.05$.

Europe PMC Funders Author Manuscripts

Europe PMC Funders Author Manuscripts

## Supplementary Material

Refer to Web version on PubMed Central for supplementary material.

## ACKNOWLEDGMENTS

We thank Cosima Zimmermann for providing HCMV stocks. This study was supported by the European Research Council under the European Union's Seventh Framework Programme (FP/2007-2013)/ERC Grant Agreement number 320473-BacNK BacNK and by the European Union FP7 grant-316655 (VACTRAIN). Additional support came from the I-CORE Program of the Planning and Budgeting Committee and the Israel Science Foundation and by the I-Core on Chromatin and RNA in Gene Regulation, the GIF Foundation, the Lewis Family Foundation, the Israel Cancer Research Fund professorship grant, the Israeli Science Foundation, the Helmholtz Israel grant and the Rosetrees Trust (all to O.M.) and VISTRIE VH-VI-242 (to H.H.). O.M. is a Crown Professor of Molecular Immunology. E.S. is supported by the Adams Fellowship Programme of the Israel Academy of Sciences and Humanities and by the Foulkes Foundation. D.S. receives funding from the People Programme (Marie Curie Actions) of the European Union's Seventh Framework Programme FP7 (FP7-PEOPLE-2012-ITN-317013).

## REFERENCES

Ashiru O, Bennett NJ, Boyle LH, Thomas M, Trowsdale J, Wills MR. NKG2D ligand MICA is retained in the cis-Golgi apparatus by human cytomegalovirus protein UL142. J. Virol. 2009; 83:12345–12354. [PubMed: 19793804]

Ashiru O, López-Cobo S, Fernández-Messina L, Pontes-Quero S, Pandolfi R, Reyburn HT, Valés-Gómez M. A GPI anchor explains the unique biological features of the common NKG2D-ligand allele MICA*008. Biochem. J. 2013; 454:295–302. [PubMed: 23772752]

Chalupny NJ, Rein-Weston A, Dosch S, Cosman D. Downregulation of the NKG2D ligand MICA by the human cytomegalovirus glycoprotein UL142. Biochem. Biophys. Res. Commun. 2006; 346:175–181. [PubMed: 16750166]

Cheent K, Khakoo SI. Natural killer cells: integrating diversity with function. Immunology. 2009; 126:449–457. [PubMed: 19278418]

Fernández-Messina L, Reyburn HT, Valés-Gómez M. Human NKG2D-ligands: cell biology strategies to ensure immune recognition. Front. Immunol. 2012; 3:299. [PubMed: 23056001]

Fielding CA, Aicheler R, Stanton RJ, Wang ECY, Han S, Seirafian S, Davies J, McSharry BP, Weekes MP, Antrobus PR, et al. Two novel human cytomegalovirus NK cell evasion functions target MICA for lysosomal degradation. PLoS Pathog. 2014; 10:e1004058. [PubMed: 24787765]

Fukami-Kobayashi K, Shiina T, Anzai T, Sano K, Yamazaki M, Inoko H, Tateno Y. Genomic evolution of MHC class I region in primates. Proc. Natl. Acad. Sci. USA. 2005; 102:9230–9234. [PubMed: 15967992]

González S, López-Soto A, Suarez-Alvarez B, López-Vázquez A, López-Larrea C. NKG2D ligands: key targets of the immune response. Trends Immunol. 2008; 29:397–403. [PubMed: 18602338]

Griffiths PD. Burden of disease associated with human cytomegalovirus and prospects for elimination by universal immunisation. Lancet Infect. Dis. 2012; 12:790–798. [PubMed: 23017365]

Halenius A, Gerke C, Hengel H. Classical and non-classical MHC I molecule manipulation by human cytomegalovirus: so many targets-but how many arrows in the quiver? Cell. Mol. Immunol. 2014; doi: 10.1038/cmi.2014.105

Hengel H, Esslinger C, Pool J, Goulmy E, Koszinowski UH. Cytokines restore MHC class I complex formation and control antigen presentation in human cytomegalovirus-infected cells. J. Gen. Virol. 1995; 76:2987–2997. [PubMed: 8847504]

Huber MTM, Tomazin R, Wisner T, Boname J, Johnson DC. Human cytomegalovirus US7, US8, US9, and US10 are cytoplasmic glycoproteins, not found at cell surfaces, and US9 does not mediate cell-to-cell spread. J. Virol. 2002; 76:5748–5758. [PubMed: 11992003]

Jones TR, Muzithras VP. Fine mapping of transcripts expressed from the US6 gene family of human cytomegalovirus strain AD169. J. Virol. 1991; 65:2024–2036. [PubMed: 1848316]

Europe PMC Funders Author Manuscripts

Jones TR, Muzithras VP. A cluster of dispensable genes within the human cytomegalovirus genome short component: IRS1, US1 through US5, and the US6 family. J. Virol. 1992; 66:2541–2546. [PubMed: 1312642]

Le VTK, Trilling M, Hengel H. The cytomegaloviral protein pUL138 acts as potentiator of tumor necrosis factor (TNF) receptor 1 surface density to enhance ULb'-encoded modulation of TNF-α signaling. J. Virol. 2011; 85:13260–13270. [PubMed: 21976655]

Loureiro J, Ploegh HL. Antigen presentation and the ubiquitin-proteasome system in host-pathogen interactions. Adv. Immunol. 2006; 92:225–305. [PubMed: 17145306]

Mandelboim O, Reyburn HT, Valés-Gómez M, Pazmany L, Colonna M, Borsellino G, Strominger JL. Protection from lysis by natural killer cells of group 1 and 2 specificity is mediated by residue 80 in human histocompatibility leukocyte antigen C alleles and also occurs with empty major histocompatibility complex molecules. J. Exp. Med. 1996; 184:913–922. [PubMed: 9064351]

Mandic L, Miller MS, Coulter C, Munshaw B, Hertel L. Human cytomegalovirus US9 protein contains an N-terminal signal sequence and a C-terminal mitochondrial localization domain, and does not alter cellular sensitivity to apoptosis. J. Gen. Virol. 2009; 90:1172–1182. [PubMed: 19264602]

McSharry BP, Burgert H-G, Owen DP, Stanton RJ, Prod'homme V, Sester M, Koebernick K, Groh V, Spies T, Cox S, et al. Adenovirus E3/19K promotes evasion of NK cell recognition by intracellular sequestration of the NKG2D ligands major histocompatibility complex class I chain-related proteins A and B. J. Virol. 2008; 82:4585–4594. [PubMed: 18287244]

Orange JS. Natural killer cell deficiency. J. Allergy Clin. Immunol. 2013; 132:515–525. [PubMed: 23993353]

Pande NT, Powers C, Ahn K, Früh K. Rhesus cytomegalovirus contains functional homologues of US2, US3, US6, and US11. J. Virol. 2005; 79:5786–5798. [PubMed: 15827193]

Pellet P, Vaneensberghe C, Debré P, Sumyuen MH, Theodorou I. MIC genes in non-human primates. Eur. J. Immunogenet. 1999; 26:239–241. [PubMed: 10331162]

Petersdorf EW, Shuler KB, Longton GM, Spies T, Hansen JA. Population study of allelic diversity in the human MHC class I-related MIC-A gene. Immunogenetics. 1999; 49:605–612. [PubMed: 10369917]

Slavuljica I, Krmpotić A, Jonjić S. Manipulation of NKG2D ligands by cytomegaloviruses: impact on innate and adaptive immune response. Front. Immunol. 2011; 2:85. [PubMed: 22566874]

Stern-Ginossar N, Elefant N, Zimmermann A, Wolf DG, Saleh N, Biton M, Horwitz E, Prokocimer Z, Prichard M, Hahn G, et al. Host immune system gene targeting by a viral miRNA. Science. 2007; 317:376–381. [PubMed: 17641203]

Stern-Ginossar N, Weisburd B, Michalski A, Le VTK, Hein MY, Huang S-X, Ma M, Shen B, Qian S-B, Hengel H, et al. Decoding human cytomegalovirus. Science. 2012; 338:1088–1093. [PubMed: 23180859]

Weekes MP, Tomasec P, Huttlin EL, Fielding CA, Nusinow D, Stanton RJ, Wang ECY, Aicheler R, Murrell I, Wilkinson GWG, et al. Quantitative temporal viromics: an approach to investigate host-pathogen interaction. Cell. 2014; 157:1460–1472. [PubMed: 24906157]

Wiertz EJ, Tortorella D, Bogyo M, Yu J, Mothes W, Jones TR, Rapoport TA, Ploegh HL. Sec61-mediated transfer of a membrane protein from the endoplasmic reticulum to the proteasome for destruction. Nature. 1996; 384:432–438. [PubMed: 8945469]

Wilkinson GW, Tomasec P, Stanton RJ, Armstrong M, Prod'homme V, Aicheler R, McSharry BP, Rickards CR, Cochrane D, Llewellyn-Lacey S, et al. Modulation of natural killer cells by human cytomegalovirus. J. Clin. Virol. 2008; 41:206–212. [PubMed: 18069056]

Zhang Y, Lazaro AM, Lavingia B, Stastny P. Typing for all known MICA alleles by group-specific PCR and SSOP. Hum. Immunol. 2001; 62:620–631. [PubMed: 11390037]

Zou Y, Bresnahan W, Taylor RT, Stastny P. Effect of human cytomegalovirus on expression of MHC class I-related chains A. J. Immunol. 2005; 174:3098–3104. [PubMed: 15728525]

Europe PMC Funders Author Manuscripts

Europe PMC Funders Author Manuscripts

## Highlights

- HCMV downregulates the highly prevalent stress-induced ligand MICA*008
- The viral US9 protein selectively targets MICA*008 to proteasomal degradation
- MICA*008 downregulation results in reduced NK cell killing during HCMV infection
- This mechanism is a viral counterstrike to the “escape variant” MICA*008

Europe PMC Funders Author Manuscripts

Europe PMC Funders Author Manuscripts

## In Brief

MICA*008 is a stress-induced ligand, long considered an “escape variant” resistant to human cytomegalovirus immune evasion mechanisms. Seidel et al. now show that the viral glycoprotein US9 specifically targets MICA*008 to proteasomal degradation, thereby hampering the elimination of cytomegalovirus-infected cells. This finding illustrates the dynamic co-evolution of host and pathogen.

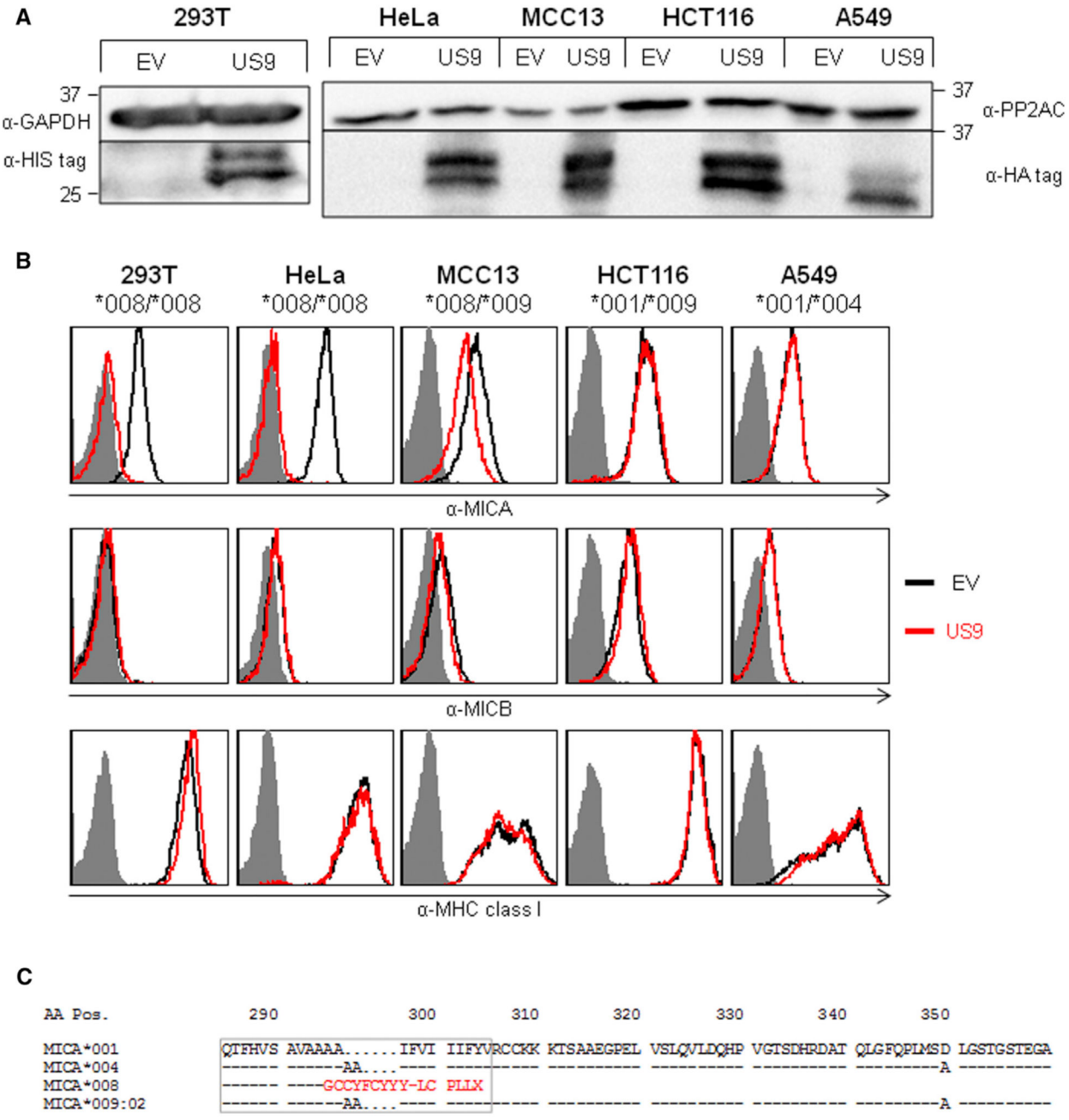


**Figure 1. US9 Expression Specifically Reduces MICA Surface Expression in Certain Cell Lines**

(A) Western blot of US9 expression in the indicated cells, transduced either with an EV or with tagged US9, using the indicated antibodies. (B) FACS staining for MICA, MICB, and MHC class I expression (top, middle, and bottom histograms, respectively) in cell lines transduced with an EV (black histograms) or with US9 (red histograms). Gray-filled histograms represent secondary antibody staining. Representative of three independent experiments. (C) Multiple sequence alignment conducted using the IMGT/HLA database (http://www.ebi.ac.uk/ipd/imgt/hla/) of the TM and cytoplasmic domain of the MICA alleles



Europe PMC Funders Author Manuscripts
Europe PMC Funders Author Manuscripts

present in the cell lines described in (B). Red highlights sequences unique for MICA*008. The gray square marks the TM region.
See also Figure S1.

Europe PMC Funders Author Manuscripts

Europe PMC Funders Author Manuscripts

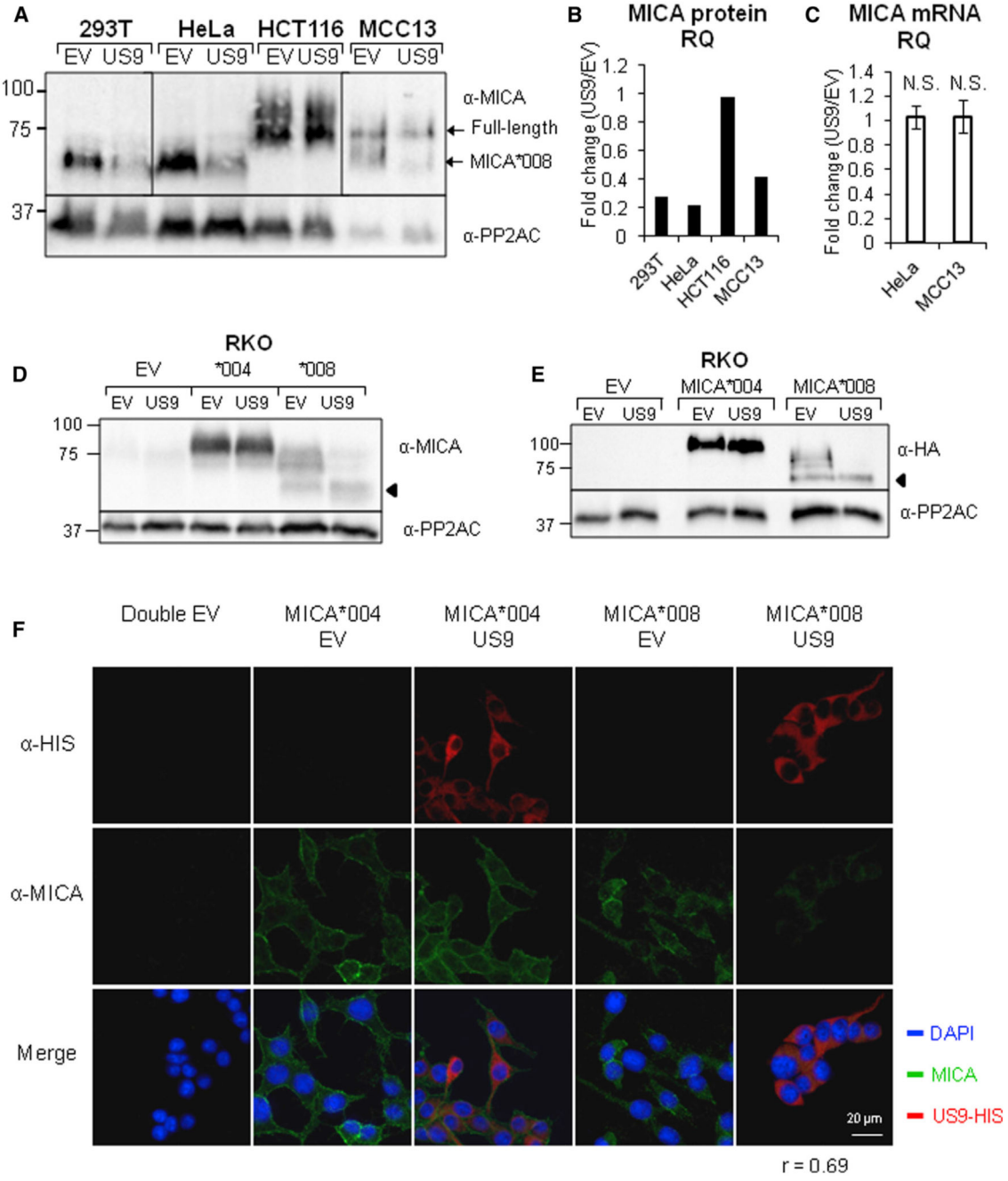


**Figure 2. US9 Regulates MICA Post-transcriptionally**

(A) Lysates obtained from the indicated cells expressing either an EV or US9 were blotted using α-MICA. α-PP2AC served as loading control. Shown are different exposures of the same gel due to differences in MICA expression levels. A single exposure can be seen in Figure S2A.

(B) Quantification of the relative MICA protein levels shown in (A): protein quantity was normalized, and then the ratio of MICA levels for each cell line was calculated as follows: (level in US9-expressing cells)/(level in EV-expressing cells).



Europe PMC Funders Author Manuscripts
Europe PMC Funders Author Manuscripts

(C) qRT-PCR was performed in triplicate using cDNA from the indicated cell lines and MICA-specific primers. The results were normalized, and then the fold change of the mRNA level was calculated for each experiment as follows: (level in US9-expressing cells)/(level in EV-expressing cells). Error bars show SEM for two to four independent experiments; p value was calculated using a single-sample t test against a hypothetical mean of 1. N.S., nonsignificant.

(D and E) Western blot using the indicated antibodies was performed on lysates obtained from RKO cells transduced with an EV, with MICA*004-HA, or with MICA*008-HA and co-transduced with an EV or with US9. α-PP2AC served as loading control. The arrows indicate the immature form of MICA*008.

(F) RKO cells as in (D) and (E) were stained with an α-MICA and an α-HIS tag antibodies, and images were captured by confocal microscopy. The average correlation coefficient for colocalization between the two antibodies is indicated, calculated for >30 cells.

See also Figure S2.

Europe PMC Funders Author Manuscripts

Europe PMC Funders Author Manuscripts

Europe PMC Funders Author Manuscripts

Europe PMC Funders Author Manuscripts

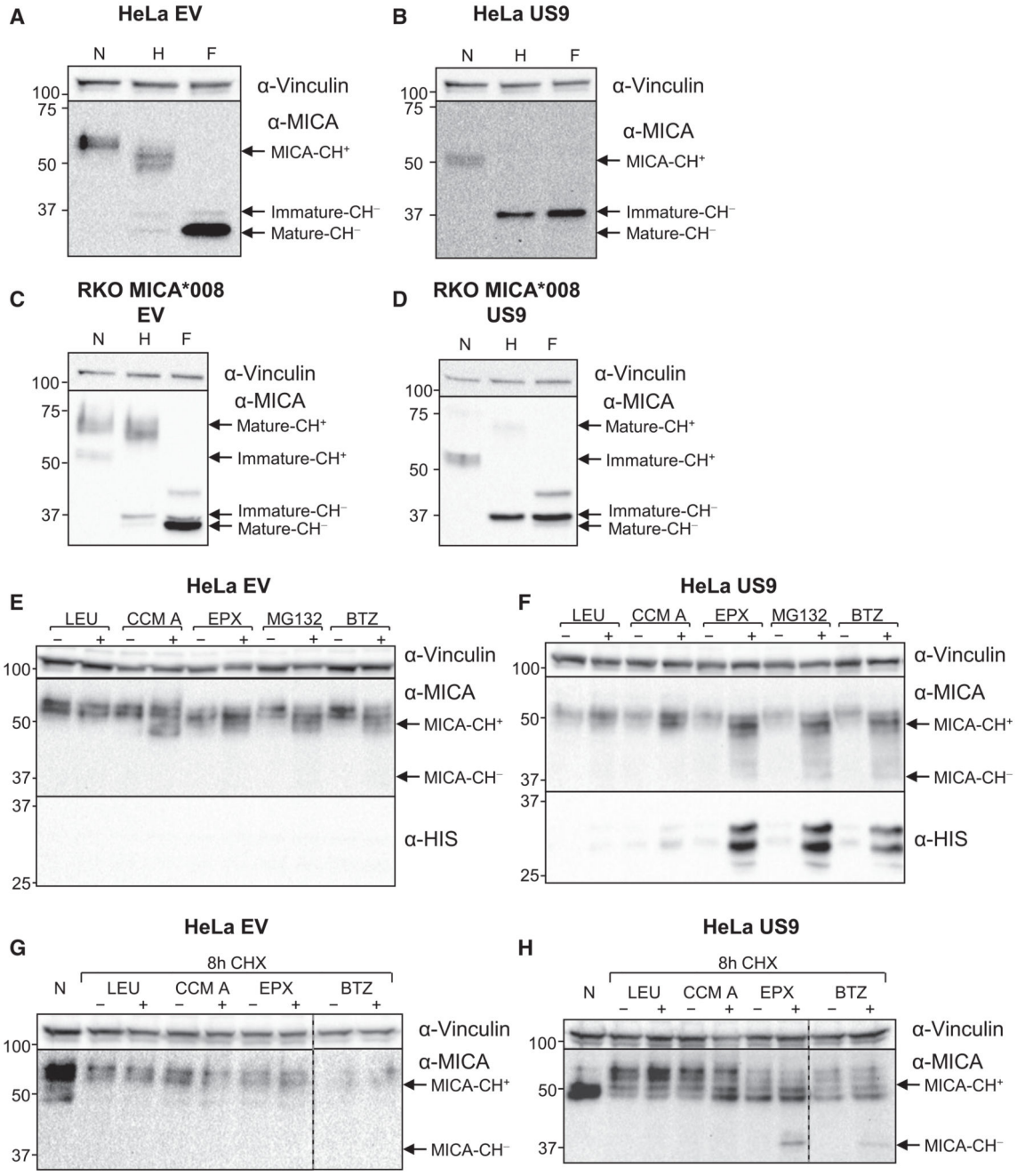


**Figure 3. US9 Targets MICA*008 to Proteasomal Degradation**

(A–D) HeLa cells expressing EV (A) or US9 (B) or RKO MICA*008-HA cells co-transduced with EV (C) or US9 (D) were lysed, and the lysates were left untreated or digested with endoH or with PNGaseF (marked N, H, and F, respectively) and then blotted using the indicated antibodies. Arrows indicate MICA forms with and without carbohydrates ($CH^{+/-}$). α-Vinculin served as loading control.

(E and F) HeLa cells expressing EV (E) or US9 (F) were mock treated or were treated with the following inhibitors: the lysosomal protease inhibitor LEU (100 μg/ml), the lysosomal

acidification inhibitor CCM A (20 nM), the irreversible proteasome inhibitor EPX (0.5 μM), the reversible proteasome inhibitor MG132 (10 μM), or the reversible proteasome inhibitor BTZ (10 μM). Following 16 hr of treatment, the cells were lysed and blotted using α-MICA and α-HIS antibodies. α-Vinculin served as loading control. Arrows indicate MICA forms with and without carbohydrates ($CH^{+/-}$).

(G and H) HeLa cells expressing EV (G) or US9 (H) were left untreated (N) or were incubated for 8 hr with the translation inhibitor CHX (100 μg/ml) in combination with mock treatment or with the following inhibitors: LEU (100 μg/ml), CCM A (40 nM), EPX (40 μM), or BTZ (300 μM). Following treatment, cells were lysed and blotted with α-MICA. α-Vinculin served as control. Arrows indicate MICA forms with and without carbohydrates (CH+/−). Dashed vertical lines indicate different gel segments.

See also Figure S3.

Europe PMC Funders Author Manuscripts

Europe PMC Funders Author Manuscripts

Europe PMC Funders Author Manuscripts

Europe PMC Funders Author Manuscripts

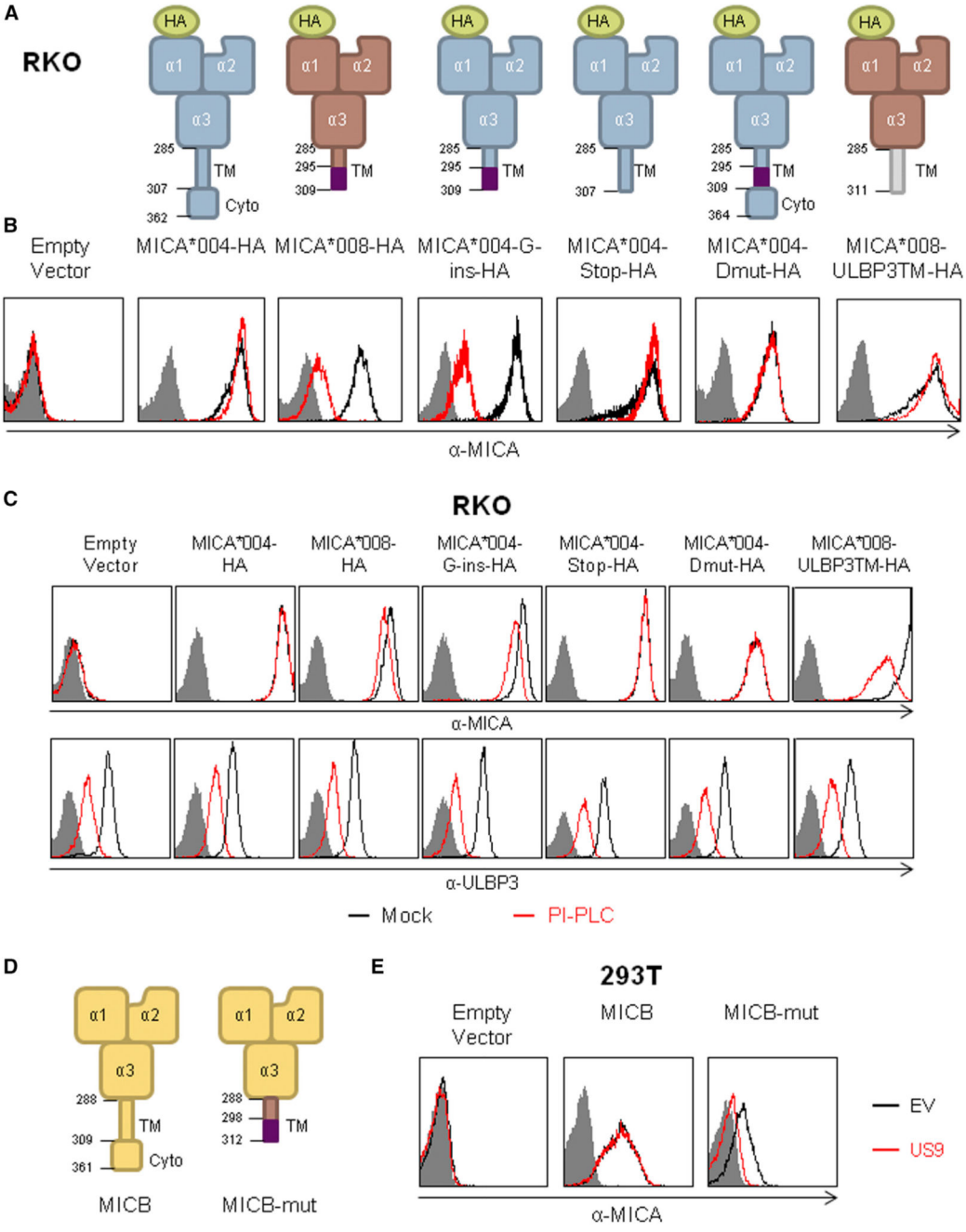


**Figure 4. Specific Features of MICA*008, Correlated with Noncanonical GPI Anchoring, Are Required for US9-Mediated Downregulation**

(A) Schematic representation of the MICA mutants and chimeric proteins used to identify which feature of MICA*008 is recognized by US9. The numbers indicate the AA position of the TM and cytoplasmic domains and the positions of the G-insert mutation, where applicable. The AA positions stated are within the mature protein, without taking into account the HA-tag sequence.

(B) FACS staining of MICA expression in RKO cells transduced with the MICA proteins described in (A) and co-transduced with an empty vector (black histogram) or with US9 (red

histogram). Grey-filled histograms represent secondary antibody staining. Representative of three independent experiments.

(C) RKO cells transduced with the indicated proteins described in (A) were mock treated (black histograms) or treated (red histograms) with PI-PLC for 2 hr and then stained for MICA (top histograms) and for ULBP3 (bottom histograms), as a positive control, and analyzed by flow cytometry. Grey-filled histograms represent secondary antibody staining. Representative of two independent experiments.

(D) Schematic representation of MICB and a mutated MICB. The numbers indicate the AA position within the mature protein of the TM and cytoplasmic domains and the positions of the G-insert mutation, where applicable.

(E) α-MICB FACS staining of 293T cells transduced with an empty vector (left histogram); with a WT MICB (middle histogram) or with MICB-mut (right) and co-transduced with an empty vector (black histogram) or with US9 (red histogram). Grey-filled histograms represent secondary antibody staining. Representative of three independent experiments. See also Figure S4.

Europe PMC Funders Author Manuscripts

Europe PMC Funders Author Manuscripts

Europe PMC Funders Author Manuscripts

Europe PMC Funders Author Manuscripts

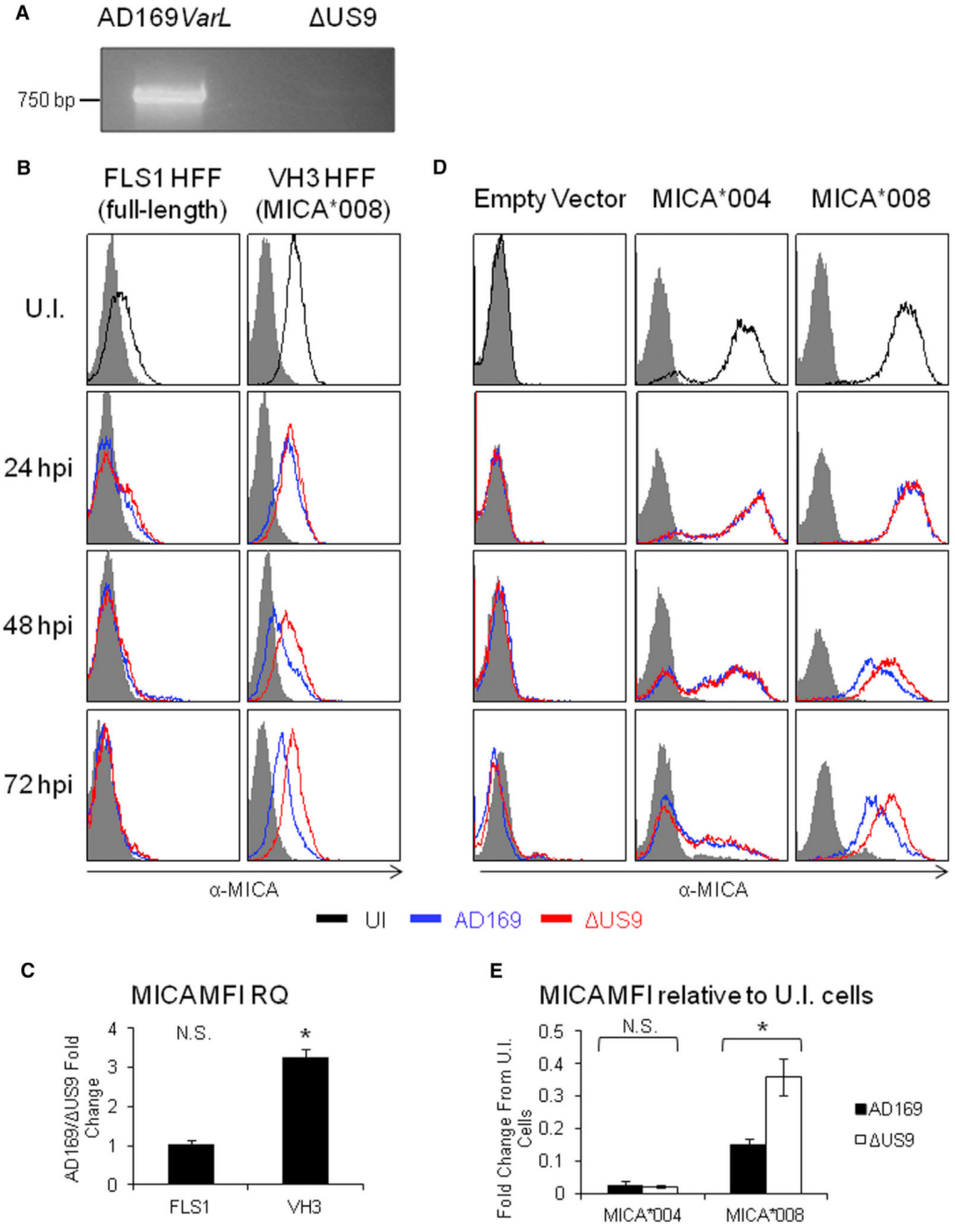


**Figure 5. US9 Reduces MICA*008 Surface Expression during HCMV Infection**

(A) PCR using US9-specific primers on viral genomic DNA derived from AD169 *VarL* and ΔUS9 virus, as annotated, resolved on acrylamide gel.

(B) FACS staining of HFF that were either UI or infected at an MOI of 2–4 with the indicated virus, at the indicated times post-infection. Black histogram, UI cells; blue histogram, AD169 *varL*; red histogram, ΔUS9. Grey-filled histograms represent isotype-matched control staining. Representative of three independent experiments.

Europe PMC Funders Author Manuscripts

Europe PMC Funders Author Manuscripts

(C) Quantification of the relative median fluorescent intensity (MFI) of MICA for the 72 hpi staining in (B) was calculated as follows: background staining was subtracted, and then the ratio (US9-expressing cells MFI)/(EV-expressing cells MFI) was calculated. Error bars show SEM for three independent experiments; p value was calculated using a single-sample t test against a hypothetical mean of 1. *$p < 0.05$. N.S, nonsignificant.

(D) FACS staining of FLS3 HFF transduced with an empty vector, MICA*004, or MICA*008 that were either UI or infected at an MOI of 2–4 with the indicated virus at the indicated times after infection. Black histogram, UI cells; blue histogram, AD169 *varL*; red histogram, ΔUS9. Grey-filled histograms represent isotype-matched control staining. Representative of three independent experiments.

(E) The relative MFI of MICA for the 72 hpi staining in (D) was calculated as follows: background staining was subtracted, and then the MFI for each virus type was normalized according to the MFI of the UI control. Error bars show SEM for three independent experiments. A Student's t test was used to compare the MFI of AD169 *varL*-infected cells versus ΔUS9-infected cells. *$p < 0.05$. N.S., nonsignificant.

See also Figure S5.

Europe PMC Funders Author Manuscripts

Europe PMC Funders Author Manuscripts

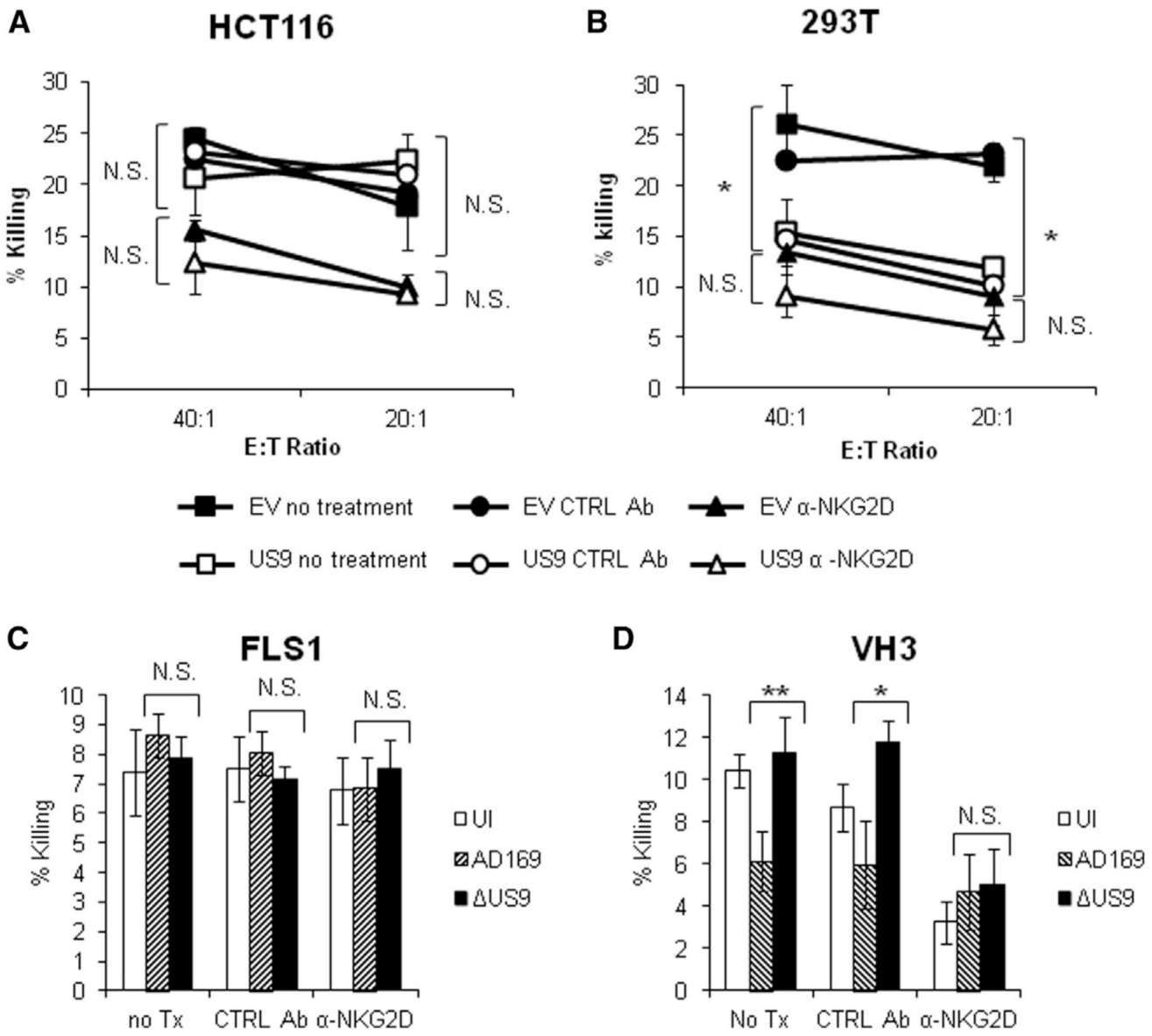


**Figure 6. The US9-Mediated Reduction of MICA*008 Leads to Reduced NKG2D-Mediated Killing**

(A and B) NK cells were untreated (squares), incubated with a control mAb (12E7; circles) or with α-NKG2D (triangles), and then incubated with HCT116 cells in (A) or with 293T cells in (B). Black-filled shapes indicate EV-expressing target cells, and white-filled shapes indicate US9-expressing target cells. Error bars represent SD. A Student's t test was performed to evaluate significance. *$p < 0.05$. N.S., nonsignificant. Representative of two independent experiments.

(C and D) NK cells were untreated, incubated for 5 hr with a control mAb (12E7) or with α-NKG2D, and then incubated overnight at an E:T ratio of 150:1 with FLS1 HFFs in (C) or with VH3 HFFs in (D).

Error bars represent SD. A Student's t test was performed to evaluate significance. *p < 0.05, **p < 0.01. N.S., nonsignificant. Representative of two independent experiments. See also Figure S6.

Europe PMC Funders Author Manuscripts

Europe PMC Funders Author Manuscripts

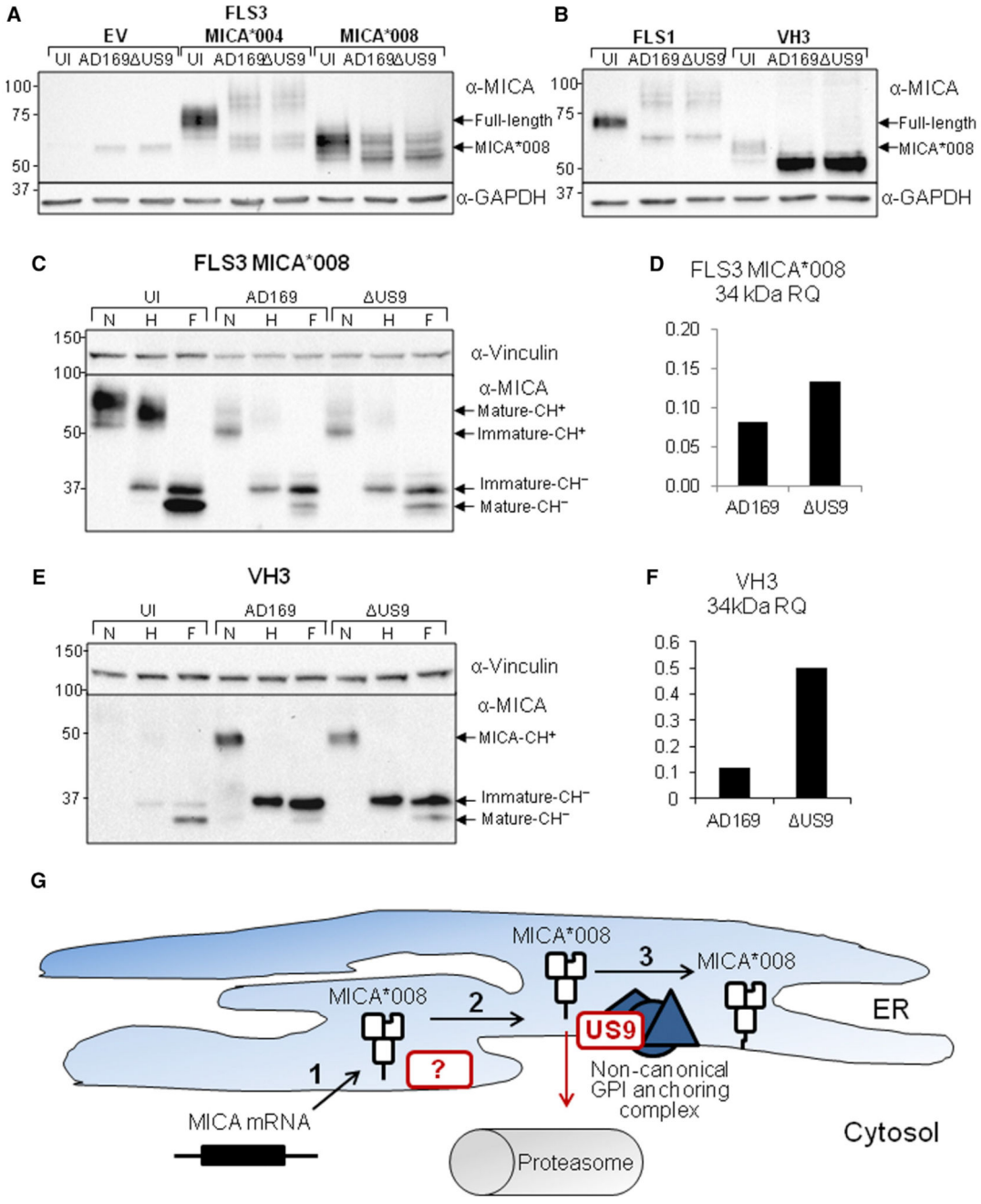


**Figure 7. US9 Reduces the Amount of GPI-Anchored MICA*008 in HCMV-Infected Cells but Does Not Affect Overall MICA*008 Levels**

(A) FLS3 HFFs transduced with an empty vector, MICA*004 or MICA*008, were either UI or infected at an MOI of 2–4 with the indicated virus and lysed 72 hpi. Western blot was performed using α-MICA antibody. α-GAPDH served as loading control.

(B) FLS1 and VH3 HFFs were either UI or infected at an MOI of 2–4 with the indicated virus and lysed 72 hpi. Western blot was performed using α-MICA antibody. α-GAPDH served as loading control.



Europe PMC Funders Author Manuscripts
Europe PMC Funders Author Manuscripts

Europe PMC Funders Author Manuscripts

Europe PMC Funders Author Manuscripts

(C) FLS3 HFF expressing MICA*008 were either UI or infected at an MOI of 2–4 with the indicated virus and lysed 72 hpi. The lysates were either untreated or digested with endoglycosidase H or with PNGase F (marked N, H, and F, respectively). Western blot was performed using α-MICA antibody. α-Vinculin served as loading control. Arrows indicate MICA forms with and without carbohydrates ($CH^{+/-}$).

(D) Quantification of the 34-kDa GPI-anchored form of MICA*008 shown in (C), normalized according to the loading control and then normalized relative to the quantity in the UI control.

(E) VH3 HFFs were UI or infected at an MOI of 2–4 with the indicated virus and lysed at 72 hpi. The lysates were untreated or digested with endoH or with PNGaseF (marked N, H, and F, respectively). Western blot was performed using α-MICA. α-Vinculin served as loading control. Arrows indicate MICA forms with and without carbohydrates ($CH^{+/-}$).

(F) Quantification of the 34 kDa GPI-anchored form of MICA*008 shown in (E), normalized according to the loading control and then normalized relative to the quantity in the UI control.

(G) A model of HCMV effect on MICA*008: (1) following HCMV infection, MICA*008 mRNA is upregulated and the protein is translated into the ER lumen. (2) MICA*008's immature, nonanchored form remains in the ER for a prolonged period, and unknown HCMV protein(s) bind and sequester it at this stage. (3) MICA*008, which has escaped other HCMV mechanisms, undergoes GPI anchoring via an unknown noncanonical pathway. US9 targets this stage and diverts MICA*008 to the cytosol, where it is subsequently degraded by the proteasome. Viral mechanisms are marked by red borders. See also Figure S6.